Nano Research 2016, 9(9): 2707–2714
DOI 10.1007/s12274-016-1159-x
Research Article

ISSN 1998-0124
CN 11-5974/O4

Ethylenediaminetetraacetic acid-assisted synthesis of Bi_2Se_3 nanostructures with unique edge sites

Xianli Liu, Zhicheng Fang, Qi Zhang, Ruijie Huang, Lin Lin, Chunmiao Ye, Chao Ma (✉), and Jie Zeng (✉)

Hefei National Laboratory for Physical Sciences at the Microscale, Key Laboratory of Strongly-Coupled Quantum Matter Physics of Chinese Academy of Sciences, Hefei Science Center & National Synchrotron Radiation Laboratory, Department of Chemical Physics, University of Science and Technology of China, Hefei 230026, China

Received: 20 March 2016
Revised: 17 May 2016
Accepted: 19 May 2016

© Tsinghua University Press and Springer-Verlag Berlin Heidelberg 2016

KEYWORDS

Bi_2Se_3,
edge sites,
ethylenediaminetetraacetic acid (EDTA),
dislocation source,
supersaturation

ABSTRACT

Nanomaterials with unique edge sites have received increasing attention due to their superior performance in various applications. Herein, we employed an effective ethylenediaminetetraacetic acid (EDTA)-assisted method to synthesize a series of exotic Bi_2Se_3 nanostructures with distinct edge sites. It was found that the products changed from smooth nanoplates to half-plate-containing and crown-like nanoplates upon increasing the molar ratio of EDTA to Bi^{3+}. Mechanistic studies indicated that, when a dislocation source and relatively high supersaturation exist, the step edges in the initially formed seeds can serve as supporting sites for the growth of epilayers, leading to the formation of half-plate-containing nanoplates. In contrast, when the dislocation source and a suitably low supersaturation are simultaneously present in the system, the dislocation-driven growth mode dominates the process, in which the step edges form at the later stage of the growth responsible for the formation of crown-like nanoplates.

1 Introduction

Topological insulators (TIs), which are bulk insulators but possess exotic metallic states on their surface, have attracted great interest due to their novel properties and promising applications [1–7]. After the discovery of topological behavior in Bi_xSb_{1-x} and related compounds [8–10], Bi_2Se_3 has emerged as the best candidate to study topological surface states due to its large band gap of approximately 0.3 eV, equivalent to 3,600 K [11, 12]. This band gap is much larger than the room-temperature energy scale, which means behavior as a TI may be observed at room temperature. However, the topological properties of Bi_2Se_3 with a high carrier density are often dominated by its bulk state [13], and so decreasing the dimension of Bi_2Se_3 towards the nanoscale to enhance surface effects is required for potential devices.

Morphological modulation has been demonstrated to be a powerful tool to tailor the physicochemical

Address correspondence to Jie Zeng, zengj@ustc.edu.cn; Chao Ma, cma@ustc.edu.cn

properties of Bi_2Se_3 nanocrystals. For example, Bi_2Se_3 exhibits a very low figure of merit (ZT) of less than 0.2 in thermoelectrical measurements, while the peak ZT for a pellet composed of single-layered nanostructures can reach 0.48, as reported by Zou and co-workers [14]. More interestingly, tuning their thickness can possibly switch Bi_2Se_3 thin films from a 3-dimensional (3D) to 2-dimensional (2D) TI phase. As such, the energy gap opening can be clearly seen by angle-resolved photoemission spectroscopy when the thickness of Bi_2Se_3 films is below six quintuple layers (QLs) [15]. In addition, by probing the transport properties of the surface states of Bi_2Se_3 nanoribbons, Cui and co-workers reported that their large surface-to-volume ratio contributes to effective suppression of the bulk effects [13]. As a result, different methods have been proposed to prepare diverse Bi_2Se_3 nanostructures such as nanorods [16], nanosheets [17, 18], nanoplates [19] and architectural nanostructures [20]. Moreover, nanomaterials with special edge sites were reported to exhibit superior performance in a series of applications [21–27]. For example, a remarkable enhancement in current was observed at the step edges compared with that on terraces of Bi_2Te_3 [28]. For spiral TIs, it has been predicted theoretically that one-dimensional topologically protected modes can exist [29]. In addition, we have not only investigated the scattering of surface states off the spiral steps, but also explored some promising applications such as Majorana fermions and quantum computing [30, 31]. Owing to the surface sensitivity of TIs, special edge sites are expected to endow Bi_2Se_3 nanostructures such as mentioned above with extraordinary properties. However, despite the success of preparing Bi_2Se_3 nanostructures with multiple morphologies, effective procedures for the synthesis of Bi_2Se_3 nanostructures with special edge sites have barely been lucubrated up to now.

Herein, we demonstrate the preparation of exotic Bi_2Se_3 nanostructures with special edge sites by introducing ethylenediaminetetraacetic acid (EDTA) in a polyol synthesis procedure. In the absence of EDTA, conventional Bi_2Se_3 nanoplates with smooth surfaces were obtained. In contrast, in the presence of EDTA (54.3 mg, corresponding to an EDTA/Bi^{3+} molar ratio of 10), products formed hexagonal nanoplates with half plates extending from their diagonal positions. When even more EDTA was introduced (108.6 mg, an EDTA/Bi^{3+} molar ratio of 20), its chelation ability became more obvious, leading to the formation of crown-like Bi_2Se_3 nanostructures.

2 Experimental

2.1 Chemicals and materials

Sodium selenite (Na_2SeO_3, 99%), bismuth nitrate pentahydrate ($Bi(NO_3)_3{\cdot}5H_2O$, 99%), EDTA, L-ascorbic acid (AA), poly(vinylpyrrolidone) (PVP, $M_W \approx 40{,}000$), ethylene glycol (EG, 99%), and HCl (38 wt.% in H_2O) were purchased from Sinopharm Chemical Reagent Co. Ltd (Shanghai, China). All chemicals were used as received without further purification.

2.2 Synthesis of Bi_2Se_3 nanostructures with different morphologies

Stoichiometric amounts of $Bi(NO_3)_3{\cdot}5H_2O$ (9 mg) and Na_2SeO_3 (4.8 mg) were dissolved separately in 0.45 mL of EG and then injected rapidly into another EG solution (14.1 mL), held at 176 °C, containing PVP (143 mg), AA (87 mg), HCl (20 μL, 11.8 M), and different amounts of EDTA powder. After the injection was finished, the reaction was allowed to proceed for 30 min. At this point, the color of the solution had turned from faint yellow to dark grey, indicating the end of the reaction and formation of Bi_2Se_3 nanocrystals. The final products were precipitated by centrifugation at 9,000 rpm for 5 min, and washed three times by ethanol at a lower centrifugation speed of 3,500 rpm for 5 min.

2.3 Instrumentation

Transmission electron microscope (TEM) images were taken using a Hitachi H-7650 microscope at an acceleration voltage of 100 kV. High-resolution TEM (HRTEM), high-angle annular dark-field scanning TEM (HAADF-STEM), and X-ray energy dispersive spectrometry (EDS) analyses were carried out on a JEOL ARM-200F field-emission TEM operating at 200 kV. Atomic force microscopy (AFM) studies were performed by means of a Veeco DI Nano-scope MultiMode V system. Scanning electron microscopy (SEM) images were obtained with a JSM-6700F operated at 5 kV. X-ray diffraction (XRD) characterization was performed using a Philips X'Pert Pro X-ray diffractometer with a monochromatized Cu Kα radiation source and wavelength of 0.1542 nm.

3 Results and discussion

3.1 Structural and compositional analysis of three types of Bi_2Se_3 nanostructures

Figure 1 shows the layered crystal structure of Bi_2Se_3, in which five covalently bonded atomic sheets (Se–Bi–Se–Bi–Se) form QLs (~1 nm each) that are linked along the z-axis via van der Waals interactions [32]. This unique feature renders the growth along the z-axis much slower than that in other directions, resulting in the preferential formation of quasi-2D plate-like structures [33].

In a typical synthesis procedure, by simply varying the amounts of EDTA added, Bi_2Se_3 nanoplates with different morphologies were obtained. Specifically, in the absence of EDTA smooth Bi_2Se_3 nanoplates were obtained in the final products (Fig. S1 in the Electronic Supplementary Material (ESM)). When 54.3 mg of EDTA (corresponding to an EDTA/Bi^{3+} molar ratio of 10) was added, hexagonal nanoplates with other half plates extending from their diagonal positions were obtained (Fig. 2(a) and Fig. S2 in the ESM). For simplicity, these products were labeled as sample A in the following context. The Moiré patterns, resulting from the overlap of two or more half plates growing in different orientations, could be clearly seen in high-magnification TEM images of an individual sample A (Figs. 2(b)–2(d)). Figures 2(e) –2(g) show SEM images of an individual sample A with either one or two half plates, respectively. Figure S3 in the ESM shows collections of other SEM images, in which the half plates were observed on both sides of the base-plate. The unique structure associated with the half plates inspired us to track the formation process of sample A. Through monitoring of the TEM images of nanocrystals obtained at different stages, we identified that small and irregular Bi_2Se_3 nanoplates were formed in the early stage. Subsequently, the oriented attachment of Bi_2Se_3 around their outer edges enlarges the nanoplates with extended half plates [34] (Fig. S4 in the ESM).

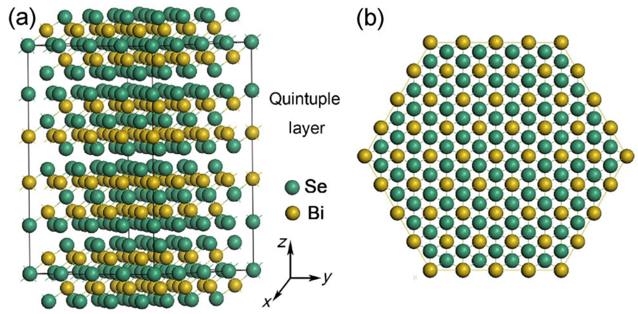

Figure 1 (a) Side view of the layered crystal structure of Bi_2Se_3. (b) Top view of the layered crystal structure of Bi_2Se_3. The yellow and green balls represent Bi and Se elements, respectively.

Figure 2(h) shows an HAADF-STEM image of an individual sample A with several half plates. No obvious defects exist at the interface between the half plates and base-plates (Fig. 2(j)). In contrast, interfaces between each two QLs with a thickness of 0.99 nm were observed at the center (Fig. 2(l)), indicating that the base-plates and half plates are connected not by van der Waals forces but via strong covalent bonds. In Fig. S5 (in the ESM), some special nanoplates are shown, in which a spiral growth track also appeared.

When the amount of EDTA was increased to 108.6 mg (corresponding to a molar ratio of EDTA/Bi^{3+} of 20), we obtained Bi_2Se_3 nanoplates with several sub-nanostructures randomly dispersed near the edges of the hexagonal nanoplates (Fig. 3(a) and Fig. S6 in the ESM). For simplicity, we defined these products as sample B. The 3D AFM image in Fig. 3(b) clearly displays an overall crown-like outline for sample B, with peripheral growth of pyramid-like sub-nanostructures. The AFM image and height profile analyses, shown in Fig. S7 (in the ESM), indicate that the thickness of the base-plate is approximately 8 nm, while the sub-nanostructures are non-uniform in height. In addition, irregular sub-nanostructures near the edges can clearly be observed in the TEM image of an individual sample B shown in Fig. S8 (in the ESM). Figures 3(c) and 3(d) are an HAADF image of the same sample, and the magnification of the region marked by a black triangle, respectively. In the sub-nanostructures, two sets of densely distributed triangular fringes, caused by the screw dislocation, were clearly observed. To better visualize the structure of such sub-nanostructures, AFM analysis was performed. As shown in Fig. S9 (in the ESM), the growth

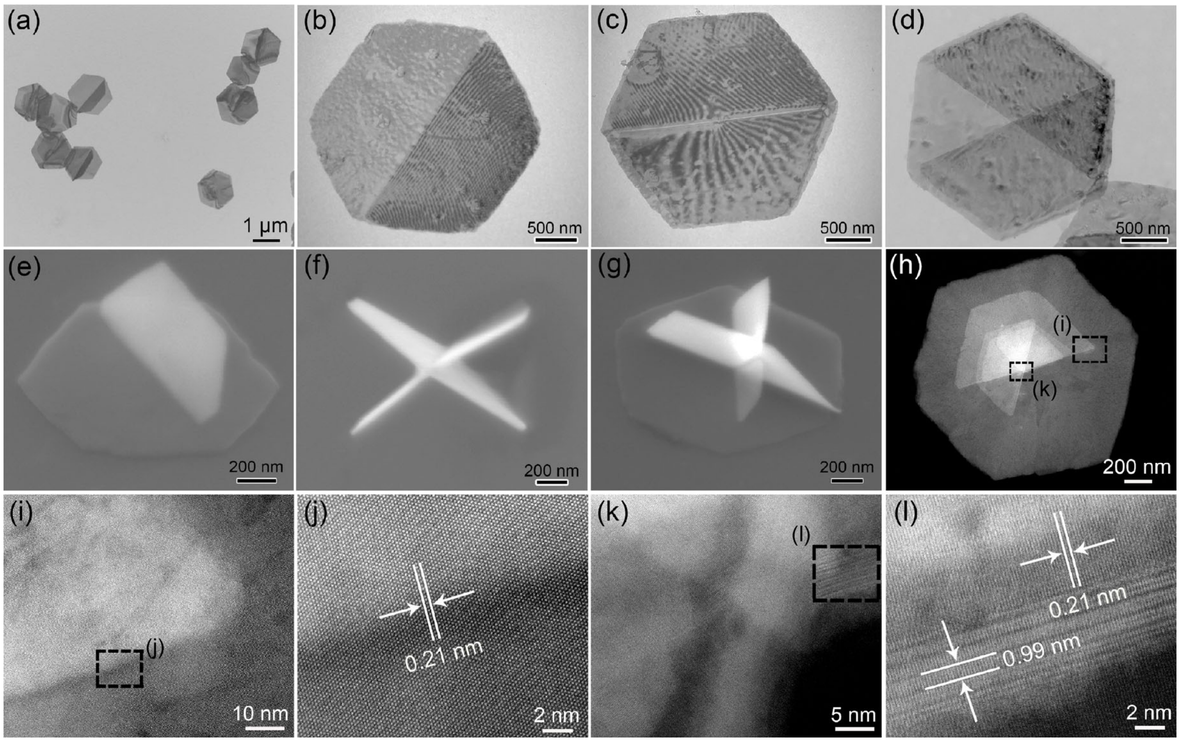

Figure 2 (a) Low-magnification TEM image of sample A. (b)–(d) TEM images of an individual sample A. (e)–(g) SEM images of an individual sample A at a titling angle of 45°. (h) HAADF image of an individual sample A. (i) and (k) Magnified HAADF images of the region shown in (h). (j) and (l) HRTEM images of the corresponding region shown in (i) and (k).

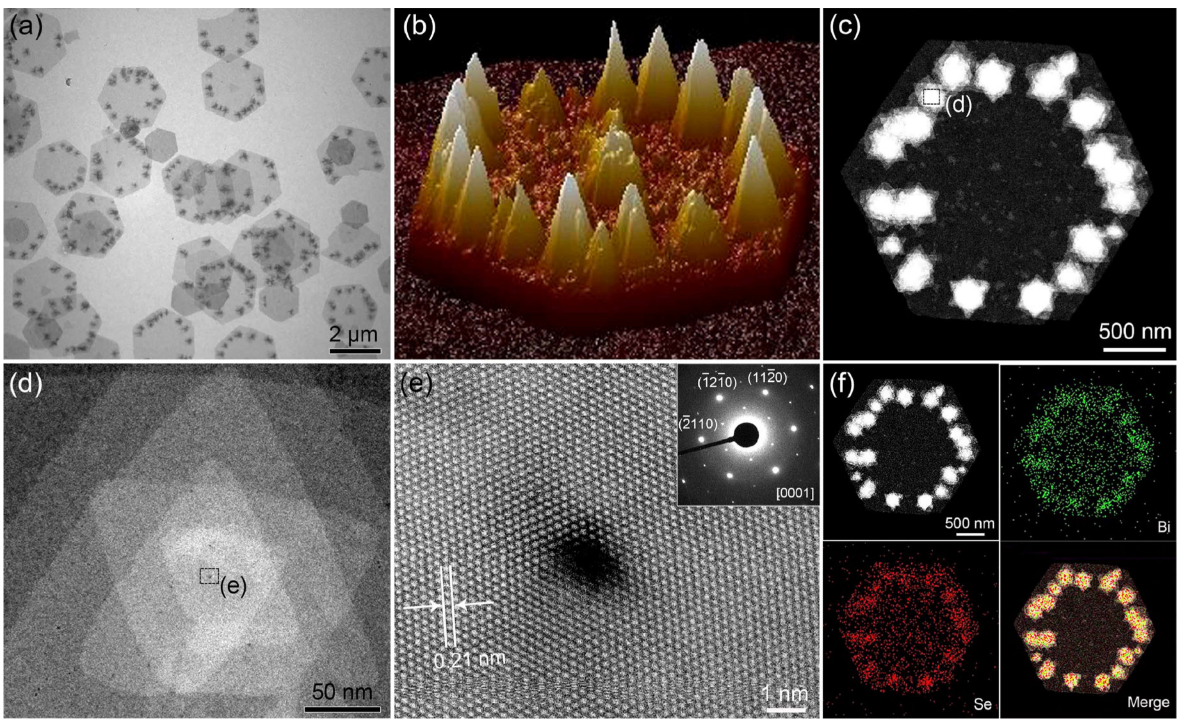

Figure 3 (a) Low-magnification TEM image of sample B. (b) Three-dimensional AFM image of an individual sample B. (c) HAADF image of an individual sample B. (d) HAADF image of a magnified sub-nanostructure. (e) HRTEM image of the region shown in (d). The corresponding selected area electron diffraction pattern is shown in the top-right inset. (f) HAADF image and STEM-EDX elemental mapping of Bi, Se, and merged images of an individual sample B.

trajectory of the pyramid-like sub-nanostructures could be clearly observed.

A hollow core exists in the center region of the sub-nanostructures (Fig. 3(e)), which is consistent with our previous work [35]. The lattice spacing of 0.21 nm corresponds to the $(11\bar{2}0)$ planes, and the selected area electron diffraction (SAED) pattern indicates the single-crystal nature of sample B. As shown in Fig. 3(f), the mapping images show the uniform distribution of Bi (green) and Se (red) elements. For characterization of the crystalline structure of both samples, X-ray diffraction (XRD) patterns are provided in Fig. S10 (in the ESM), indicating a rhombohedral crystalline structure (JCPDS No. 89-2008; a = 4.139 Å, c = 28.636 Å). It should be noted that the (006) and (0, 0, 15) diffraction peaks of both samples were much stronger than the standard ones, which can be attributed to the enhancement of the diffraction in the vertical direction (z-axis). In addition, some differences exist between the diffraction peaks of both samples, possibly due to their anisotropic structures.

3.2 Formation mechanism of different Bi_2Se_3 nanostructures

From the above analysis, it is evident that the molar ratio between EDTA and Bi^{3+} plays a vital role in determining the morphology of the final samples. When the molar ratio between EDTA and Bi^{3+} was increased from 0 to 10 and 20, the products changed from smooth nanoplates to samples A and B, respectively (Fig. 4). It is known that EDTA generally serves as a chelating agent that can bind to metal cations through two amines and four carboxyl groups [36]. Formed complexes can dissociate and release metal ions reversibly into the reaction solution, which has an inevitable impact on the atomic binding rate. The EDTA-assisted route has been used before to prepare Bi_2WO_6 multilayered disc-like and 3D hierarchical nest-like architectures with a defect-rich state, in which the electrostatic effect and hydrogen bonds facilitate self-aggregation and assembly of the formed particles [37]. In our synthesis, EDTA-derived chelating resulted in a relatively slower growth rate, concluded from the tinctorial changes during the reaction. When more EDTA was added into the system, it took longer for the solution's color to change from faint yellow to dark grey.

Typically, crystal formation takes place in two stages: initial nucleation and subsequent growth. In solutions, where particles are free to move, smooth nanoplates follow an oriented attachment mechanism, which involves spontaneous self-organization of adjacent particles. Accordingly, they aggregate at a planar interface with a common crystallographic orientation [38]. However, in the presence of EDTA, the growth mode is different. The role of EDTA can be understood from two aspects. On the one hand, most Bi^{3+} ions will immediately interact with EDTA molecules upon the addition of precursors, greatly decreasing the concentration of free Bi^{3+} ions during the nucleation stage. On the other hand, these EDTA molecules will partially absorb on the surface of Bi_2Se_3 nuclei, which may change the surface energy of different sites and generate necessary steric hindrance for the following attachment of Bi_2Se_3. In the case of sample A, random and imperfect attachment of Bi_2Se_3 particles was expected to induce dislocation during the nucleation stage. Previously, our group reported a screw-dislocation-driven growth of spiral-type Bi_2Se_3 nanoplates at a relatively low supersaturation [39]. In contrast, the supersaturation in the current condition failed to maintain a relatively low level due to the interactions between Bi^{3+} ions and EDTA. As a result, dislocation served as step edges for planar extension to induce the growth of half plates, rather than support the formation of spiral-type nanoplates. Just as the Jin group reported, two basic ingredients, a screw dislocation source and a suitably low supersaturation condition, are required to promote dislocation-driven growth [40]. In order to elucidate the role of EDTA, we further decreased the amount of EDTA to 27.1 mg, with the other conditions unchanged. In this system, a mixture of smooth nanoplates and sample A was formed in the resultant product (Fig. S11 in the ESM), which can be considered a transition stage from smooth nanoplates to sample A. To elucidate the formation mechanism of sample B, a series of TEM images was taken from samples obtained at different time points, shown in Fig. S12 (in the ESM). Irregular nanosheets were formed in the initial stage with many Bi_2Se_3 nanoparticles around. The subsequent attachment of those Bi_2Se_3 particles evolved the nanosheets into

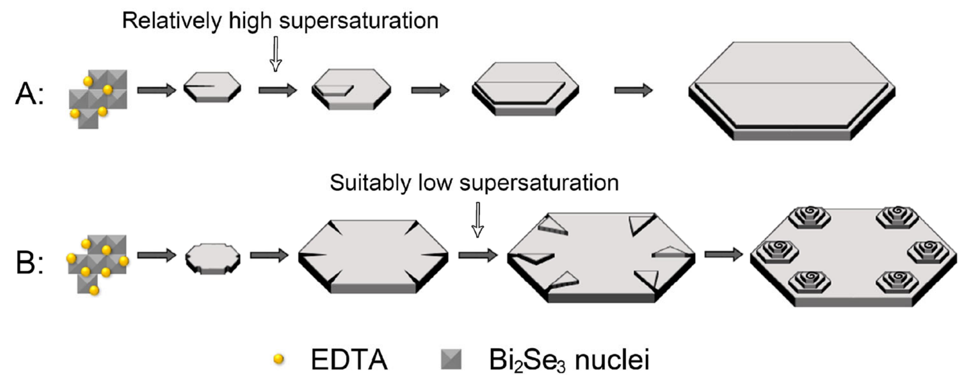

Figure 4 Schematic illustration of the proposed formation mechanism of two samples. The yellow balls represent EDTA molecules, and the grey squares represent Bi_2Se_3 nuclei.

incipient hexagonal nanoplates [34]. It should be noted that the surfaces are quite rough, with many defects at all times. Crystals grow from a screw dislocation and undergo continuous development at two competitive rates, an in-plane rate and a vertical rate. When the driving force of the reaction system decreases to a critical level, the vertical rate disappears [21]. With the reaction ongoing, those defective sites function as slip planes for the dislocation-driven growth under the decreasing supersaturation condition. During the subsequent growth, there are always step edges present to which atoms can be added, and thus Bi_2Se_3 particles are continuously deposited along them. However, at this time, the precursors will mostly have been used already, so the subsequent reaction will consume the remaining precursors quickly and terminate the growth. Taken together, the above-mentioned results in the formation of Bi_2Se_3 nanoplates with spiral-type sub-nanostructures.

4 Conclusions

In summary, an effective EDTA-assisted approach was employed to synthesize exotic Bi_2Se_3 nanostructures with special edge sites. It was found that the morphology varied remarkably when adding different relative amounts of EDTA to the reaction system. Specifically, the mechanistic studies indicate that, when a dislocation source exists under a relatively high supersaturation condition, the step edges could serve as supporting sites for the growth of epilayers. In contrast, crystal growth would take place as dislocation-driven spiral growth only when the two basic conditions, involving the presence of a dislocation source and suitably low supersaturation, were met. This inspiring work provides a simple way to obtain exotic Bi_2Se_3 nanomaterials with unique edge sites, and will hopefully be extended to the preparation of other two-dimensional materials for practical applications.

Acknowledgements

This work was supported by Collaborative Innovation Center of Suzhou Nano Science and Technology, the National Basic Research Program of China (No. 2014CB932700), National Natural Science Foundation of China (Nos. 21573206, 51371164, and 51132007), Strategic Priority Research Program B of the CAS (No. XDB01020000), Hefei Science Center CAS (No. 2015HSC-UP016), and Fundamental Research Funds for the Central Universities.

Electronic Supplementary Material: Supplementary material (TEM and SEM images of smooth Bi_2Se_3 nanoplates, SEM images of sample A, TEM images of sample A obtained at different reaction time points, SEM, TEM, and HAAFD images of an individual sample A, SEM image of sample B, AFM analysis of sample B, TEM image of an individual sample B, AFM analysis of an individual sub-nanostructure on sample B, XRD patterns of samples A and B, TEM images of the sample obtained by adding 27.1 mg of EDTA with the other conditions unchanged, and TEM images of sample B obtained at different reaction time points) is available in the online version of this article at http://dx.doi.org/10.1007/s12274-016-1159-x.

References

[1] Moore, J. E. The birth of topological insulators. *Nature* **2010**, *464*, 194–198.

[2] Hasan, M. Z.; Kane, C. L. Topological insulators. *Rev. Mod. Phys.* **2010**, *82*, 3045–3067.

[3] Kong, D. S.; Cui, Y. Opportunities in chemistry and materials science for topological insulators and their nanostructures. *Nat. Chem.* **2011**, *3*, 845–849.

[4] Müchler, L.; Casper, F.; Yan, B. H.; Chadov, S.; Felser, C. Topological insulators and thermoelectric materials. *Phys. Status Solidi (RRL)* **2013**, *7*, 91–100.

[5] Qi, X. L.; Zhang, S. C. Topological insulators and superconductors. *Rev. Mod. Phys.* **2011**, *83*, 1057–1110.

[6] Taskin, A. A.; Sasaki, S.; Segawa, K.; Ando, Y. Achieving surface quantum oscillations in topological insulator thin films of Bi_2Se_3. *Adv. Mater.* **2012**, *24*, 5581–5585.

[7] Peng, H. L.; Dang, W. H.; Cao, J.; Chen, Y. L.; Wu, D.; Zheng, W. S.; Li, H.; Shen, Z. X.; Liu, Z. F. Topological insulator nanostructures for near-infrared transparent flexible electrodes. *Nat. Chem.* **2012**, *4*, 281–286.

[8] Fu, L.; Kane, C. L. Topological insulators with inversion symmetry. *Phys. Rev. B* **2007**, *76*, 045302.

[9] Hsieh, D.; Qian, D.; Wray, L.; Xia, Y.; Hor, Y. S.; Cava, R. J.; Hasan, M. Z. A topological Dirac insulator in a quantum spin Hall phase. *Nature* **2008**, *452*, 970–974.

[10] Hsieh, D.; Xia, Y.; Wray, L.; Qian, D.; Pal, A.; Dil, J. H.; Osterwalder, J.; Meier, F.; Bihlmayer, G.; Kane, C. L. et al. Observation of unconventional quantum spin textures in topological insulators. *Science* **2009**, *323*, 919–922.

[11] Zhang, H. J.; Liu, C. X.; Qi, X. L.; Dai, X.; Fang, Z.; Zhang, S. C. Topological insulators in Bi_2Se_3, Bi_2Te_3 and Sb_2Te_3 with a single Dirac cone on the surface. *Nat. Phys.* **2009**, *5*, 438–442.

[12] Xia, Y.; Qian, D.; Hsieh, D.; Wray, L.; Pal, A.; Lin, H.; Bansil, A.; Grauer, D.; Hor, Y. S.; Cava, R. J. et al. Observation of a large-gap topological-insulator class with a single Dirac cone on the surface. *Nat. Phys.* **2009**, *5*, 398–402.

[13] Peng, H. L.; Lai, K. J.; Kong, D. S.; Meister, S.; Chen, Y. L.; Qi, X. L.; Zhang, S. C.; Shen, Z. X.; Cui, Y. Aharonov-Bohm interference in topological insulator nanoribbons. *Nat. Mater.* **2010**, *9*, 225–229.

[14] Hong, M.; Chen, Z. G.; Yang, L.; Han, G.; Zou, J. Enhanced thermoelectric performance of ultrathin Bi_2Se_3 nanosheets through thickness control. *Adv. Electron. Mater.* **2015**, *1*, 1500025.

[15] Zhang, Y.; He, K.; Chang, C. Z.; Song, C. L.; Wang, L. L.; Chen, X.; Jia, J. F.; Fang, Z.; Dai, X.; Shan, W. Y. et al. Crossover of the three-dimensional topological insulator Bi_2Se_3 to the two-dimensional limit. *Nat. Phys.* **2010**, *6*, 584–588.

[16] Xu, S.; Zhao, W. B.; Hong, J. M.; Zhu, J. J.; Chen, H. Y. Photochemical synthesis of Bi_2Se_3 nanosphere and nanorods. *Mater. Lett.* **2005**, *59*, 319–321.

[17] Min, Y.; Moon, G. D.; Kim, B. S.; Lim, B.; Kim, J. S.; Kang, C. Y.; Jeong, U. Quick, controlled synthesis of ultrathin Bi_2Se_3 nanodiscs and nanosheets. *J. Am. Chem. Soc.* **2012**, *134*, 2872–2875.

[18] Sun, L. P.; Lin, Z. Q.; Peng, J.; Weng, J.; Huang, Y. Z.; Luo, Z. Q. Preparation of few-layer bismuth selenide by liquid-phase-exfoliation and its optical absorption properties. *Sci. Rep.* **2014**, *4*, 4794.

[19] Zhang, J.; Peng, Z. P.; Soni, A.; Zhao, Y. Y.; Xiong, Y.; Peng, B.; Wang, J. B.; Dresselhaus, M. S.; Xiong, Q. H. Raman spectroscopy of few-quintuple layer topological insulator Bi_2Se_3 nanoplatelets. *Nano Lett.* **2011**, *11*, 2407–2414.

[20] Sun, Z. L.; Liufu, S.; Chen, X. H.; Chen, L. D. Controllable synthesis and electrochemical hydrogen storage properties of Bi_2Se_3 architectural structures. *Chem. Commun.* **2010**, *46*, 3101–3103.

[21] Ni, B.; Wang, X. Edge overgrowth of spiral bimetallic hydroxides ultrathin-nanosheets for water oxidation. *Chem. Sci.* **2015**, *6*, 3572–3576.

[22] Tao, C. G.; Jiao, L. Y.; Yazyev, O. V.; Chen, Y. C.; Feng, J. J.; Zhang, X. W.; Capaz, R. B.; Tour, J. M.; Zettl, A.; Louie, S. G. et al. Spatially resolving edge states of chiral graphene nanoribbons. *Nat. Phys.* **2011**, *7*, 616–620.

[23] Nakada, K.; Fujita, M.; Dresselhaus, G.; Dresselhaus, M. S. Edge state in graphene ribbons: Nanometer size effect and edge shape dependence. *Phys. Rev. B* **1996**, *54*, 17954–17961.

[24] Wang, X. R.; Ouyang, Y. J.; Jiao, L. Y.; Wang, H. L.; Xie, L. M.; Wu, J.; Guo, J.; Dai, H. J. Graphene nanoribbons with smooth edges behave as quantum wires. *Nat. Nanotechnol.* **2011**, *6*, 563–567.

[25] Xie, J. F.; Zhang, H.; Li, S.; Wang, R. X.; Sun, X.; Zhou, M.; Zhou, J. F.; Lou, X. W.; Xie, Y. Defect-rich MoS_2 ultrathin nanosheets with additional active edge sites for enhanced electrocatalytic hydrogen evolution. *Adv. Mater.* **2013**, *25*, 5807–5813.

[26] Zhu, W. L.; Zhang, Y. J.; Zhang, H. Y.; Lv, H. F.; Li, Q.; Michalsky, R.; Peterson, A. A.; Sun, S. H. Active and selective conversion of CO_2 to CO on ultrathin Au nanowires. *J. Am. Chem. Soc.* **2014**, *136*, 16132–16135.

[27] Xu, G.; Wang, J.; Yan, B. H.; Qi, X. L. Topological superconductivity at the edge of transition-metal dichalcogenides. *Phys. Rev. B* **2014**, *90*, 100505.

[28] Macedo, R. J.; Harrison, S. E.; Dorofeeva, T. S.; Harris, J. S.; Kiehl, R. A. Nanoscale probing of local electrical characteristics on MBE-grown Bi_2Te_3 surfaces under ambient conditions. *Nano Lett.* **2015**, *15*, 4241–4247.

[29] Ran, Y.; Zhang, Y.; Vishwanath, A. One-dimensional topologically protected modes in topological insulators with lattice dislocations. *Nat. Phys.* **2009**, *5*, 298–303.

[30] Hao, G. L.; Qi, X.; Fan, Y. P.; Xue, L.; Peng, X. Y.; Wei, X. L.; Zhong, J. X. Spiral growth of topological insulator Sb_2Te_3 nanoplates. *Appl. Phys. Lett.* **2013**, *102*, 013105.

[31] Liu, Y.; Weinert, M.; Li, L. Spiral growth without dislocations: Molecular beam epitaxy of the topological insulator Bi_2Se_3 on epitaxial graphene/SiC(0001). *Phys. Rev. Lett.* **2012**, *108*, 115501.

[32] Wyckoff, R. W. G. *Crystal Structures*, 2nd ed.; Krieger: Malabar, FL, USA, 1986.

[33] Hauer, B.; Saltzmann, T.; Simon, U.; Taubner, T. Solvothermally synthesized Sb_2Te_3 platelets show unexpected optical contrasts in mid-infrared near-field scanning microscopy. *Nano Lett*. **2015**, *15*, 2787–2793.

[34] Manna, G.; Bose, R.; Pradhan, N. Photocatalytic Au-Bi_2S_3 heteronanostructures. *Angew. Chem., Int. Ed.* **2014**, *53*, 6743–6746.

[35] Zhuang, A. W.; Li, J. J.; Wang, Y. C.; Wen, X.; Lin, Y.; Xiang, B.; Wang, X. P.; Zeng, J. Screw-dislocation-driven bidirectional spiral growth of Bi_2Se_3 nanoplates. *Angew. Chem., Int. Ed.* **2014**, *126*, 6543–6547.

[36] Feitosa, A. V.; Miranda, M. A. R.; Sasaki, J. M.; Araújo-Silva, M. A. A new route for preparing CdS thin films by chemical bath deposition using EDTA as ligand. *Braz. J. Phys*. **2004**, *34*, 656–658.

[37] Xu, L.; Yang, X. Y.; Zhai, Z.; Hou, W. H. EDTA-mediated shape-selective synthesis of Bi_2WO_6 hierarchical self-assemblies with high visible-light-driven photocatalytic activities. *CrystEngComm* **2011**, *13*, 7267–7275.

[38] Penn, R. L.; Banfield, J. F. Imperfect oriented attachment: Dislocation generation in defect-free nanocrystals. *Science* **1998**, *281*, 969–971.

[39] Liu, X. L.; Xu, J. W.; Fang, Z. C.; Lin, L.; Qian, Y.; Wang, Y. C.; Ye, C. M.; Ma, C.; Zeng, J. One-pot synthesis of Bi_2Se_3 nanostructures with rationally tunable morphologies. *Nano Res.* **2015**, *8*, 3612–3620.

[40] Hacialioglu, S.; Meng, F.; Jin, S. Facile and mild solution synthesis of Cu_2O nanowires and nanotubes driven by screw dislocations. *Chem. Commun*. **2012**, *48*, 1174–1176.